

# Reverse Polarization Switching in Ferroelectric Lead Zirconate Titanate (PZT) Thin Films

William S. Oates

Florida A & M and Florida State University, Department of Mechanical Engineering,  
Tallahassee, FL, USA

## ABSTRACT

The effect of shear stress on polarization retention in ferroelectric thin films was assessed using a nonlinear finite element phase field model. It is shown that reverse switching can occur when tetragonal phase films are grown in the (111) direction. The effect of a substrate and a top electrode are modeled by applying rigid constraints and shear loads to the finite element phase field model to predict the evolution of ferroelectric domain structures. The residual shear stress in the film is shown to increase when the film is rigidly clamped to a substrate. When shear stress is applied to the top surface of the thin film model,  $90^\circ$  domain walls move in the direction of shear loading. Model predictions are found to qualitatively correlate with piezoelectric response microscopy experiments given in the literature.

**Keywords:** ferroelectric, thin films, phase field, finite element

## 1. INTRODUCTION

Ferroelectric materials exhibit changes in polarization from an applied stress and conversely, changes in shape from an applied electric field.<sup>1</sup> On the microscopic scale, these materials are characterized by domain structures that contain regions of uniform polarization and have a length scale that is typically  $\leq 1\mu\text{m}$ . In bulk ferroelectric ceramics and single crystals, the underlying domain structures are often smeared to estimate macroscopic changes in polarization and deformation from applied stresses and electric fields. These models range from micromechanics to phenomenological continuum models and use different approximations to correlate the underlying domain structures with macroscopic thermodynamic state variables.<sup>2-4</sup> As the size of the ferroelectric structure or device converges to the micron scale, interactions among the finite number of domains becomes important. Therefore, a strong understanding of domain structures and interactions with electrode or substrate interfaces become critical to facilitate the design of ferroelectric micron and nanoscale structures and devices. This has implications on a number of applications including nonvolatile memory,<sup>5,6</sup> MEMS-based piezoelectric resonant mode cantilevers,<sup>7</sup> and microscale ultrasonic transducers for tissue ablation.<sup>8</sup>

An extensive amount of research has focused on modeling and experimental characterization of ferroelectric thin films.<sup>9-19</sup> In these structures, constraints from a substrate can play a critical role in the formation of domain patterns. For example, a model of ferroelastic epilayers on a paraelastic substrate was developed to show that refined domain patterns form as the excess surface energy increases.<sup>20</sup> Romanov et al.<sup>12</sup> modeled tetragonal phase domain structures in ferroelectric films grown in the (111) orientation. Compatible domain patterns were identified and energetics associated with different defects were quantified. In comparison to theory, several piezoelectric response microscopy (PFM) measurements have been conducted to visualize and control polarization under time varying electric fields; see<sup>17-19</sup> for examples. In particular, unusual polarization switching was observed in lead zirconate-lead titanate (PZT 40/60) thin film capacitor islands.<sup>17</sup> Reverse polarization switching occurred when a biased field was removed from ferroelectric thin films epitaxially grown in the (111) orientation. Reverse switching did not occur when the films were grown in the (001) orientation.

A mechanism for reverse switching is proposed here and validated using a finite element phase field model. The model is used to show that shear stress can lead to reverse polarization switching in tetragonal phase

---

Further author information: (Send correspondence to W.S.O.)  
W.S.O.: E-mail: woates@eng.fsu.edu, Telephone: 1 850 410 6190

ferroelectric films grown in the (111) orientation. The switching mechanism is shown to be strongly related to crystal orientation and charge compatibility along domain walls. In Section 2, the thin film domain structure is presented to motivate the reverse polarization switching problem. In Section 3, the governing equations describing the ferroelectric phase field model are given. In Section 4, the model is implemented numerically in a two-dimensional nonlinear finite element model. Domain patterns and domain wall energy are first quantified under zero stress and short circuit conditions. Shear stress is then applied to the model to simulate domain wall motion. Concluding remarks are given in Section 5.

## 2. FERROELECTRIC THIN FILM STRUCTURE

The spontaneous deformation and polarization in ferroelectric materials is governed by charge and strain compatibility. This gives rise to domain walls on certain crystallographic planes. The possible domain wall configurations in ferroelectric crystals are well-known.<sup>21</sup> In tetragonal phase ferroelectric thin films grown the (111) orientation, domain walls can be classified into two groups as described by Romanov et al.<sup>12</sup> In these thin films, the domain walls are oriented either perpendicular to the substrate or at an angle of  $\simeq 35^\circ$ . In the former, the out-of-plane polarization component alternates between each domain which gives an “unpoled” state. Conversely, a poled state forms when the domain wall angle is at  $\simeq 35^\circ$ . These two configurations are illustrated in Figure 1.

The two groups of domain patterns that can form in tetragonal phase films grown in the (111) orientation are shown in Figure 1. The ferroelectric domain configuration illustrated in Figure 1(a) is chosen for the finite element analysis. Typically, these films are grown at temperatures above the Curie temperature and then cooled prior to applying a top electrode. The paraelectric to ferroelectric phase transformation can lead to large electrostatic fields as polarization forms in the film. Therefore, the domain configuration in Figure 1(a) is energetically favorable relative to the case in Figure 1(b) prior to applying a top electrode. This as-grown state has also been confirmed experimentally using piezoelectric response microscopy.<sup>22</sup>

Elastic constraints from a substrate or top electrode can affect polarization retention in these films. When the domain pattern illustrated in Figure 1(a) is constrained to a flat substrate, residual shear stress increases. Additional mechanical constraints from a top electrode may also occur during ferroelectric switching. For example, consider an electric field that is applied to the initial domain configuration in Figure 1(a). This results predominantly in  $90^\circ$  switching. This switching behavior leads to changes in shear strain and residual shear stress when external substrate or electrode constraints are present. A schematic of the switching behavior and changes in residual shear stress are illustrated in Figure 2. As the applied electric field is reduced to zero, residual elastic energy can lead to *ferroelastic* (stress-induced) polarization switching. If the residual elastic energy is larger than some critical energy barrier, polarization switching will occur in the reverse direction anti-parallel to the applied field. Polarization switching will occur in this direction due to the effect of charge compatibility along domain walls. This behavior is simulated using a ferroelectric phase field model presented in the following sections.

## 3. PHASE FIELD MODEL GOVERNING EQUATIONS

The ferroelectric phase field model employs mechanical equilibrium, Gauss’ law, and the time dependent Ginzburg-Landau equations to quantify domain structures as a continuum.<sup>23-25</sup> The energy terms that give rise to microscale polarization and domain formation include a multiple-well Landau-Devonshire free energy<sup>26</sup> and dipole-dipole energy which is correlated with gradients in the polarization order parameter.<sup>27</sup> The minimization of free energy leads to a finite number of domains oriented in certain crystallographic orientations that is governed by strain compatibility, charge compatibility, and boundary conditions.

The Helmholtz energy density for the ferroelectric material is

$$\psi = \psi(D_i, P_i, P_{i,j}, \varepsilon_{ij}) \quad (1)$$

where  $D_i$  is electric displacement,  $P_i$  is polarization,  $P_{i,j}$  is the gradient of polarization, and  $\varepsilon_{ij}$  is infinitesimal strain. The energy function is formulated for quasi-static, isothermal processes. Indicial notation is used where summation is implied over repeated indices.

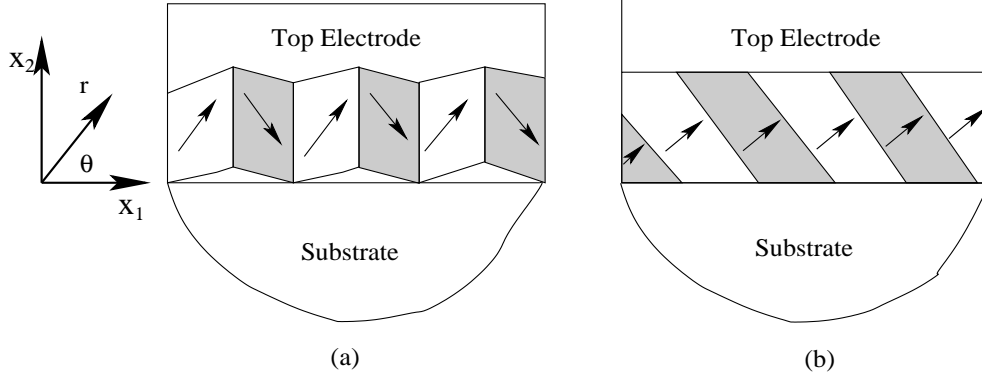


Figure 1. Cross section view of tetragonal domain structures grown in the (111) orientation. The arrows represent the in-plane polarization components and the shaded domains correspond to domains with alternating out-of-plane polarization components. Relaxed domain structures are shown which leads to “puckered” domains in the “unpoled” state in (a). When the domain walls are  $\simeq 35^\circ$  relative to the substrate, the polarization normal to the film is uniform.<sup>12</sup> The polarization direction may also be oriented  $180^\circ$  to the direction shown in the schematic.

As noted above, the Helmholtz energy is normally divided into energy components that contribute to elastic energy, electro-mechanical coupling, domain wall energy, and electrostatic energy.<sup>23, 25, 28</sup> The polarization order parameter and polarization gradients enter into the material description through the Landau-Devonshire free energy and approximation of dipole-dipole energy. The general form of the Helmholtz energy is

$$\begin{aligned} \psi = & a_{ijkl} P_{i,j} P_{k,l} + \frac{1}{2} a_{ij} P_i P_j + \frac{1}{4} a_{ijkl} P_i P_j P_k P_l + \frac{1}{6} a_{ijklmn} P_i P_j P_k P_l P_m P_n \\ & + \frac{1}{2} q_{ijkl} \varepsilon_{ij} P_k P_l + \frac{1}{2} c_{ijkl} \varepsilon_{ij} \varepsilon_{kl} + \frac{1}{2\varepsilon_0} (D_i - P_i) (D_i - P_i) \end{aligned} \quad (2)$$

where the first term is based on dipole-dipole or “exchange” energy which penalizes large gradients in the polarization order parameter. In general, the exchange parameter  $a_{ijkl}$  is a fourth order tensor; however, here this parameter will be approximated as a scalar quantity. This parameter is used in subsequent sections to

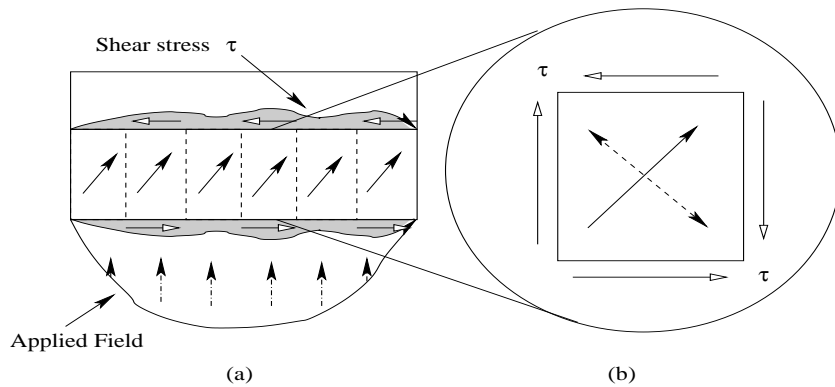


Figure 2. The schematic in (a) illustrates a monodomain with an external electric field present. The dotted lines in (a) represent the initial domain walls prior to applying a field based on the as-grown state in Figure 1(a). Changes in residual shear stress due to  $90^\circ$  switching are shown in (a). The ideal case of a single domain under pure shear is shown in (b). The dotted arrows represent the possible directions of switching; however, polarization is expected to switch towards the substrate due to charge compatibility from neighboring domains.

approximate the size and energy of a  $90^\circ$  domain wall. The second, third, and fourth terms correspond to the Landau energy expanded up to sixth order on the polarization order parameter. The fifth and sixth terms are electro-mechanical and elastic energy contributions, respectively. The electrostrictive coefficients are  $q_{ijkl}$  and the elastic modulus coefficients are  $c_{ijkl}$ . The last term is electro-static energy in free space where  $\epsilon_0$  is the permittivity of free space. The expanded form of this energy description is given in the Appendix for the two dimensional case numerically implemented in the following section.

A Legendre transformation is introduced so that the electric potential is an independent variable. This facilitates finite element implementation in Section 4 so that a single degree of freedom (i.e., electric potential) is incorporated into the nodal degrees of freedom.<sup>29</sup> The isothermal electric Gibbs energy is

$$g_2(P_i, P_{i,j}, \varepsilon_{ij}, E_i) = \psi - E_i D_i \quad (3)$$

where the electric field is defined by  $E_i = -\phi_{,i}$  and  $\phi$  is the electric potential. Infinitesimal strain  $\varepsilon_{ij} = \frac{1}{2}(u_{i,j} + u_{j,i})$  has been used where  $u_i$  is the displacement.

A kinetic law is introduced by including a dissipative potential within the energy description

$$\Pi(P_i, P_{i,j}, \dot{P}_i, \varepsilon_{ij}, E_i) = g_2(P_i, P_{i,j}, \varepsilon_{ij}, E_i) + \psi_D(\dot{P}_i). \quad (4)$$

The dissipative potential is assumed to be a quadratic function of the polarization rate,  $\psi_D(\dot{P}_i) = \beta_{ij} \dot{P}_i \dot{P}_j$ . The inverse mobility tensor,  $\beta_{ij}$ , is a second order tensor that must be positive definite based on the Clausius-Duhem inequality.<sup>25,30</sup> In Section 4, the inverse mobility is numerically implemented as  $\beta_{ij} = \beta \delta_{ij}$  where  $\delta_{ij}$  is the Kronecker delta.

The variation of (4) gives

$$\delta \Pi = \frac{\partial \Pi}{\partial P_i} \delta P_i + \frac{\partial \Pi}{\partial P_{i,j}} \delta P_{i,j} + \frac{\partial \Pi}{\partial \dot{P}_i} \delta \dot{P}_i + \frac{\partial \Pi}{\partial u_{i,j}} \delta u_{i,j} + \frac{\partial \Pi}{\partial \phi_{,j}} \delta \phi_{,j}. \quad (5)$$

Using calculus of variations and integration by parts, the relation in (5) leads to three sets of governing equations

$$\begin{aligned} \frac{\partial}{\partial x_j} \left( \frac{\partial \Pi}{\partial P_{i,j}} \right) - \frac{\partial \Pi}{\partial P_i} &= \beta_{ij} \dot{P}_j \\ \frac{\partial}{\partial x_j} \left( \frac{\partial \Pi}{\partial u_{i,j}} \right) &= \sigma_{ji,j} = 0 \\ -\frac{\partial}{\partial x_j} \left( \frac{\partial \Pi}{\partial \phi_{,j}} \right) &= D_{j,j} = 0 \end{aligned} \quad (6)$$

where (6)<sub>1</sub> is the time-dependent Ginzburg-Landau equation, (6)<sub>2</sub> is mechanical equilibrium (neglecting body forces) where  $\sigma_{ij}$  is stress and (6)<sub>3</sub> is charge compatibility where the charge density has been assumed to be zero.

#### 4. FINITE ELEMENT IMPLEMENTATION

The equations that define the ferroelectric phase field model are written in the weak form and implemented in a commercial finite element package, COMSOL. For the two dimensional problem considered here, the weak form of (6) is

$$\begin{aligned}
\int_{\Omega} \left( \beta_{ij} \dot{P}_j + \eta_i - \xi_{ji,j} \right) \delta P_i dA &= \int_{\Gamma} \xi_{ji} n_j \delta P_i dS \\
\int_{\Omega} \sigma_{ji,j} \delta u_i dA &= \int_{\Gamma} t_i \delta u_i dS \\
\int_{\Omega} D_{i,i} \delta \phi dA &= \int_{\Gamma} -\omega \delta \phi dS
\end{aligned} \tag{7}$$

where  $i, j = 1, 2$ . The area  $A$  is defined over  $\Omega$  and the boundary  $S$  is defined over  $\Gamma$ . Traction and surface charge on the boundary are denoted by  $t_i = \sigma_{ji} n_j$  and  $\omega$ , respectively. The unit normal on the boundary is denoted by  $n_i$ . The polarization gradient normal to the boundary,  $\xi_{ji} n_j$ , is set to zero in all subsequent calculations.

#### 4.1 Numerical Implementation

The finite element model is formulated for two domains separated by a  $90^\circ$  domain wall. A change in the crystal orientation is included in the model by rotating the polarization order parameter. This is done to quantify the effect of external mechanical loads when the ferroelectric thin film is grown in different crystal orientations relative to the substrate. For the two dimensional case considered here, the polarization is rotated by  $\theta = 45^\circ$  based on the coordinate system in Figure 1 to simulate in-plane behavior of the (111) orientation. The polarization is rotated according to

$$\begin{bmatrix} \bar{P}_1 \\ \bar{P}_2 \end{bmatrix} = \begin{bmatrix} \cos(\theta) & \sin(\theta) \\ -\sin(\theta) & \cos(\theta) \end{bmatrix} \begin{bmatrix} P_1 \\ P_2 \end{bmatrix} \tag{8}$$

where  $\theta$  corresponds to the angle between the material coordinates and the laboratory coordinates as previously shown in Figure 1. A substitution of  $\bar{P}_i$  into (2) gives rise to a set of material parameters that are functions of  $\theta$ . In general, the strain must be rotated also. However, in the model considered here, the elastic and electrostrictive material properties are assumed to be isotropic to simplify the free energy description. The form of the material coefficients in the rotated coordinate system are equivalent to the ones given by Zhang and Bhattacharya<sup>31</sup> and omitted here for brevity. The two dimensional form of the free energy and parameter values used in the model are given in the Appendix. The values given in Table 1 were based on parameters given by Pertsev et al.<sup>11</sup> for lead titanate. The exchange parameter was  $a_0 = 8 \times 10^{-11} \text{Vm}^3/\text{C}$  which gives a domain wall width of  $\sim 3$  nm. The domain wall energy is quantified by  $\gamma = \int_{-\infty}^{\infty} (\psi(x_1) - \psi(\infty)) dx_1$ . The energy of an unconstrained  $90^\circ$  domain wall was calculated to be  $24 \text{ mJ/m}^2$  which correlates reasonably well with *ab initio* results<sup>32</sup> and similar continuum phase field results.<sup>25</sup>

An illustration of the finite element mesh, initial domain structure, and boundary conditions are shown in Figure 3. The boundary conditions considered include 1) the traction free case, 2) clamping on the bottom surface ( $u_2 = 0$ ), and 3) applied shear stress on the top surface. The model was short circuited in all simulations. End effects are neglected by extending the model to a sufficient length in the  $x_1$  direction. Long range electrostatic effects near the ends are avoided by applying  $\omega = P_i n_i$  along these boundaries. An initial  $90^\circ$  domain pattern is assumed and the model is run for several time steps until the structure relaxes into an equilibrium state.

Simulation results for  $90^\circ$  domain structure are given in Figure 4 for the fully relaxed case and clamped conditions on the bottom surface. The shear stress ( $\sigma_{12}$ ) and polarization direction (arrows) are shown where in Figure 4(a) the fully relaxed structure is given. A ‘‘puckered’’ shape similar to the schematic in Figure 1 is shown. Additionally, shear stress concentrations are shown near the domain wall along the free surfaces. It should be noted that along the top surface, the shear stress opposes the polarization direction and therefore provides nucleation sites for reverse switching. In comparison, Figure 4(b) illustrates significant increases in residual shear stress. Here, the model has been constrained by restricting  $u_2 = 0$  on the bottom surface. Again, the sign of the shear stress opposes the polarization direction in both domains as similarly shown previously in the Figure 2(b) schematic.

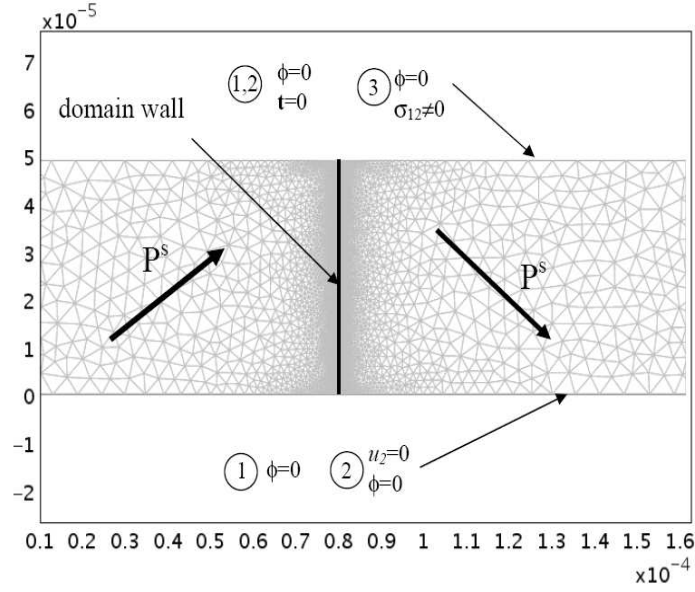


Figure 3. Representation of the finite element model used to quantify ferroelectric domain wall behavior. The mesh density is shown with a refined mesh near the domain wall ( $\sim 10$  elements over the domain wall). The material coordinates are rotated by  $\theta = 45^\circ$  to investigate  $90^\circ$  domain walls in the (11) orientation. The length units are given in millimeters.

### 4.2 Ferroelastic Reverse Switching Simulations

The effect of external mechanical loads in a ferroelectric thin film are presented here to illustrate how shear stress plays a role in reverse switching behavior. The ferroelectric model is again constrained by  $u_2 = 0$  along the

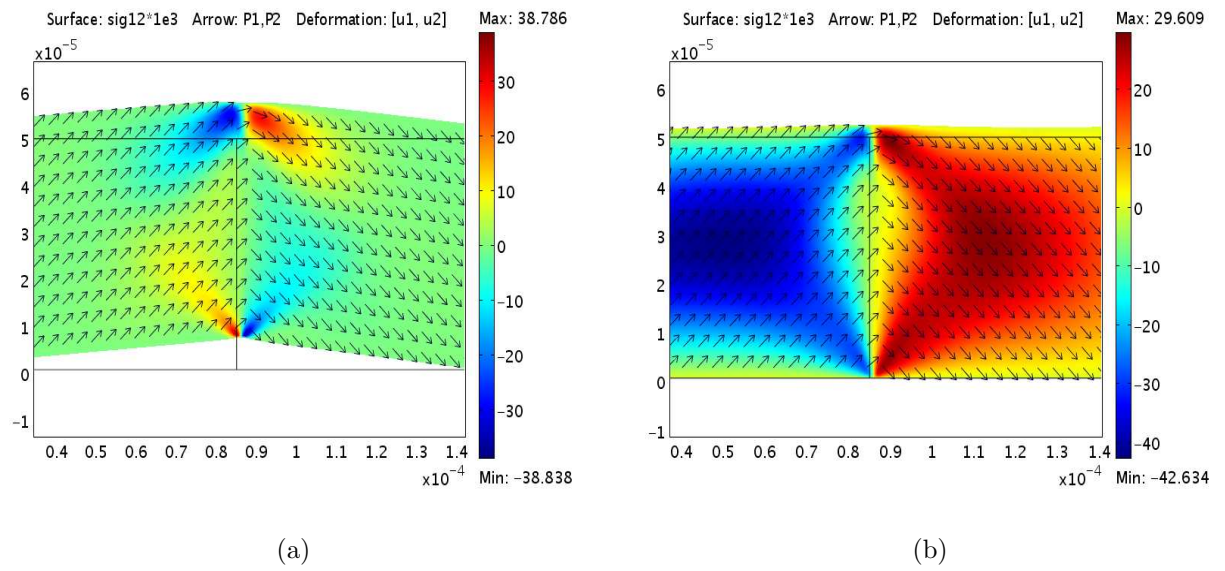


Figure 4. Finite element results of a  $90^\circ$  domain wall where shear stress is shown in MPa and the arrows represent the polarization direction. In (a), the fully relaxed case is shown with zero traction and no constraints. In (b), the bottom surface has been constrained to  $u_2 = 0$  to simulate clamping from a substrate.

bottom surface to model substrate clamping as previously illustrated by the results in Figure 4(b). In addition, a uniform shear stress is applied to the top surface. The  $90^\circ$  domain wall illustrated in Figure 4(b) is used as initial conditions for the simulations.

Simulation results in Figure 5(a) illustrate that a negative shear stress forces the domain wall to move in the direction of the applied load. The average internal shear stress increases by approximately an order of magnitude before the domain wall begins to move. Similar behavior occurs for a positive shear stress where the domain moves in the positive  $x_1$  direction. The change in the domain wall location for positive and negative shear is shown in Figure 5(b). This illustrates how shear stress may lead to reverse switching in micrometer size ferroelectric thin films.

In contrast to these simulations, thin films grown in the (001) direction will result in predominantly  $180^\circ$  switching from applied fields and no change in spontaneous strain. Therefore, reverse switching is not expected to occur in the (001) orientation as experimentally observed by Stolichnov et al.<sup>17</sup> Conversely,  $90^\circ$  switching from an electric field is energetically favorable in films grown in the (111) direction which will induce remanent shear strain and residual shear stress if a substrate or top electrode constraint is present. Applied electric fields may overcome the internal residual stress and lead to poled films when the biased field is present. Once the field is removed, residual shear stress can provide a sufficient driving force for domains to reorient in the opposite direction of the applied field.

## 5. CONCLUDING REMARKS

The in-plane behavior of domain structures in ferroelectric thin films oriented in the (111) was simulated using a nonlinear finite element phase field model. Polarization switching behavior under applied fields is proposed to create internal residual shear stress when a substrate and a top electrode are present. The finite element model was used to simulate this behavior near a  $90^\circ$  domain wall. Shear stress concentrations were found near free surfaces in an unconstrained ferroelectric film. When the bottom surface of the film was constrained in the  $x_2$  direction, shear stress increased through the film thickness. Lastly, the model illustrates that applied shear

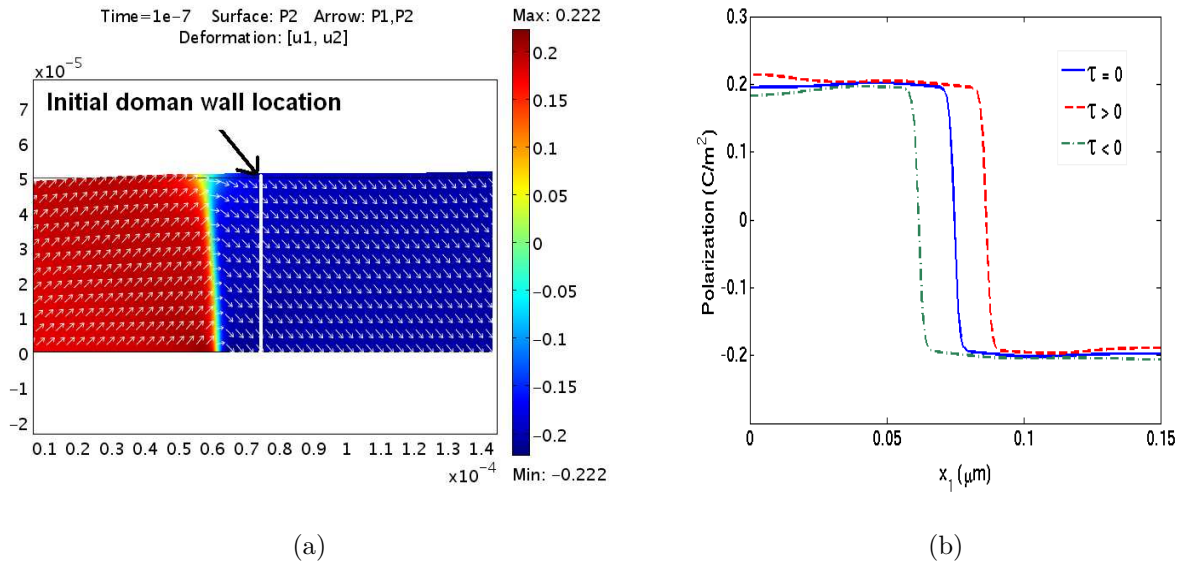


Figure 5. Simulations of domain wall motion when a shear stress is applied to the top surface of the model. In (a), the polarization component  $P_2$  is shown while applying a negative shear stress. The domain wall, originally in the center, moves in the negative  $x_1$  direction. Similarly in (b), the change in polarization component  $P_2$  along  $x_1$  is shown through the mid thickness of the thin film model which illustrates that the domain wall moves in the direction of shear stress. Here the shear stress is labeled as  $\tau$ .

stress along the top surface of the film can lead to reverse polarization switching in ferroelectric thin films grown in the (111) orientation. This behavior is due to both the shear stress direction and charge compatibility along domain walls. It should also be noted that size effects in thin film capacitor islands and top electrode geometry will lead to certain magnitudes and distributions of stress across a ferroelectric / electrode interface. Size effects and corresponding changes in driving forces that promote reverse switching in ferroelectric capacitor islands will be summarized in a future manuscript.

## APPENDIX A. FREE ENERGY PARAMETERS

The two dimensional form of the free energy given by (2) are expanded here and material parameters are quantified in Table 1.

$$\begin{aligned} \psi = & a_0(P_{1,1}^2 + P_{1,2}^2 + P_{2,1}^2 + P_{2,2}^2) + \frac{1}{2}a_1(P_1^2 + P_2^2) + a_{11}(P_1^4 + P_2^4) + a_{12}(P_1^2P_2^2) + a_{111}(P_1^6 + P_2^6) \\ & + a_{112}(P_1^4P_2^2 + P_1^2P_2^4) - \frac{q_1}{2}(\varepsilon_{11}P_1^2 + \varepsilon_{22}P_2^2) - \frac{q_2}{2}(\varepsilon_{11}P_2^2 + \varepsilon_{22}P_1^2) + q_3(\varepsilon_{12} + \varepsilon_{21})P_1P_2 \\ & + \frac{1}{2}c_{11}(\varepsilon_{11}^2 + \varepsilon_{22}^2) + \frac{1}{2}c_{12}(\varepsilon_{11}\varepsilon_{22}) + c_{66}\varepsilon_{12}^2 + \frac{1}{2\varepsilon_0} \left[ (D_1 - P_1)^2 + (D_2 - P_2)^2 \right]. \end{aligned} \quad (9)$$

where the elastic properties have been assumed to be isotropic and Voigt notation has been. The values for these parameters are given in Table 1. Moreover, the electrostrictive parameters have been restricted to  $q_3 = (q_1 - q_2)/2$ . This simplifies the model when the finite element coordinates are rotated to model the (11) orientation.

Table 1. Free energy parameters based on values given by Pertsev et al.<sup>11</sup> for lead titanate.

$a_0$	$8 \times 10^{-11} \text{Vm}^3/\text{C}$	$a_1$	$2.805 \times 10^7 \text{Vm}/\text{C}$
$a_{11}$	$-5.4 \times 10^8 \text{Vm}^5/\text{C}^3$	$a_{12}$	$4.9 \times 10^8 \text{Vm}^5/\text{C}^3$
$a_{111}$	$6.6 \times 10^9 \text{Vm}^9/\text{C}^5$	$a_{112}$	$2.9 \times 10^9 \text{Vm}^9/\text{C}^5$
$q_1$	$4 \times 10^9 \text{Nm}^2/\text{C}$	$q_2$	$-1 \times 10^9 \text{Nm}^2/\text{C}$
$q_3$	$2.5 \times 10^9 \text{Nm}^2/\text{C}$	$c_{11}$	138.5 GPa
$c_{12}$	43.3 GPa	$c_{66}$	95.2 GPa
$\varepsilon_0$	$8.85 \times 10^{-12} \text{C}/\text{mV}$	$\beta$	$1.4 \times 10^{-1} \text{Vsm}/\text{C}$

## ACKNOWLEDGMENTS

The author gratefully acknowledges discussions with Dr. Alexei Gruverman (University of Nebraska) who introduced the author to this problem. Several discussions with Dr. Gruverman were immensely helpful in shaping this work.

## REFERENCES

1. M. Lines and A. Glass, *Principles and Applications of Ferroelectrics and Related Materials*, Clarendon Press, Oxford, 1977.
2. J. Huber, N. Fleck, C. Landis, and R. McMeeking, "A constitutive model for ferroelectric polycrystals," *J. Mech. Phys. Solids* **47**(8), pp. 1663–1697, 1999.
3. M. K. and Q. Jiang, "A constitutive model for ferroelectric PZT ceramics under uniaxial loading," *Smart Mater. Struct.* **8**, pp. 441–459, 1999.
4. W. Chen and C. Lynch, "A micro-electro-mechanical model for polarization switching of ferroelectric materials," *Acta. Mater.* **48**(15), pp. 5303–5311, 1998.

5. J. Scott, F. Morrison, M. Miyake, and P. Zubko, "Nano-ferroelectric materials and devices," *Ferroelectrics* **336**, pp. 237–245, 2006.
6. J. Scott, "Applications of modern ferroelectrics," *Science* **315**, pp. 954–959, 2007.
7. J. Yi, W. Shih, R. Mutharasan, and W.-H. Shih, "In situ cell detection using piezoelectric lead zirconate titanate-stainless steel cantilevers," *J. Appl. Phys.* **93**(1), pp. 619–625, 2003.
8. O. Al-Bantaineh, R. Meyer, R. Newnham, and N. B. Smith, "Utilization of the high-frequency piezoelectric ceramic hollow spheres for expositometry and tissue ablation," *Proc. IEEE Ultrasonic Symposium*, pp. 1473–1476, 2002.
9. Y. Li, S. Hu, Z. Liu, and L. Chen, "Effect of substrate constraint on the stability and evolution of ferroelectric domain structures in thin films," *Acta. Mater.* **50**, pp. 395–411, 2002.
10. Y. Li, S. Hu, Z. Liu, and L. Chen, "Phase-field model of domain structures in ferroelectric thin films," *Appl. Phys. Lett.* **78**, pp. 3878–3880, 2001.
11. N. Pertsev, A. Zembilgotov, and A. Tagantsev, "Effect of mechanical boundary conditions on phase diagrams of epitaxial ferroelectric thin films," *Phys. Rev. Lett.* **80**(2), pp. 1988–1991, 1998.
12. A. Romanov, A. Vojta, W. Pompe, M. Lefevre, and J. Speck, "Domain patterns in (111) oriented tetragonal ferroelectric films," *Phys. Stat. Sol. (a)* **172**, pp. 225–253, 1999.
13. S. Oh and H. Jang, "Two-dimensional thermodynamic theory of epitaxial  $\text{Pb}(\text{Zr},\text{Ti})\text{O}_3$  thin films," *Phys. Rev. B* **62**(22), pp. 14757–14765, 2000.
14. W. Pompe, X. Gong, Z. Suo, and J. Speck, "Elastic energy release due to domain formation in the strained epitaxy of ferroelectric and ferroelastic films," *J. Appl. Phys.* **74**(10), pp. 6012–6019, 1993.
15. J. Scott, F. Morrison, M. Miyake, P. Zubko, X. Lou, V. Kugler, S. Rio, M. Zhang, T. Tatsuta, O. Tsuji, and T. Leedham, "Recent materials characterizations of [2d] and [3d] thin film ferroelectric structures," *J. Am. Ceram. Soc.* **88**(7), pp. 1691–1701, 2005.
16. V. Nagarajan, A. Roytburd, A. Stanishevsky, S. Prasertchoung, T. Zhao, L. Chen, J. Melngailis, O. Auciello, and R. Ramesh, "Dynamics of ferroelastic domains in ferroelectric thin films," *Nat. Mater.* **2**, pp. 43–47, 2002.
17. I. Stolichnov, E. Colla, A. Tagantsev, S. Bharadwaja, J. Cross, and M. Tsukada, "Unusual size effect on the polarization patterns in micron-size  $\text{Pb}(\text{Zr},\text{Ti})\text{O}_3$  film capacitors," *Appl. Phys. Lett.* **80**(25), pp. 4804–4806, 2002.
18. V. Shvartsman, N. Pertsev, J. Herrero, C. Zaldo, and A. Kholkin, "Nonlinear local piezoelectric deformation in ferroelectric thin films studied by scanning force microscopy," *J. Appl. Phys.* **97**, pp. 104105–1–104105–11, 2005.
19. O. Kolosov, A. Gruverman, J. Hatano, K. Takahashi, and H. Tokumoto, "Nanoscale visualization and control of ferroelectric domains by atomic force microscopy," *Phys. Rev. Lett.* **74**(21), pp. 4309–4312, 1995.
20. Y. Gao and Z. Suo, "Domain dynamics in a ferroelastic epilayer on a paraelastic substrate," *ASME Trans. Appl. Mech.* **69**, pp. 419–424, 2002.
21. J. Fousek and V. Janovec, "The orientation of domain walls in twinned ferroelectric crystals," *J. Appl. Phys.* **40**(1), pp. 135–142, 1969.
22. A. Gruverman, unpublished data.
23. H.-L. Hu and L. Chen, "Phase-field simulations of ferroelectric/ferroelastic polarization switching," *Acta. Mater.* **52**(3), pp. 749–764, 2004.
24. W. Zhang and K. Bhattacharya, "A computational model of ferroelectric domains: Part I: model formulation and domain formation," *Acta Mater.* **53**(1), pp. 185–198, 2005.
25. Y. Su and C. Landis, "Continuum thermodynamics of ferroelectric domain evolution: Theory, finite element implementation, and application to domain wall pinning," *J. Mech. Phys. Solids* **55**, pp. 280–305, 2007.
26. A. Devonshire, "Theory of barium titanate—Part I," *Phil. Mag* **40**, pp. 1040–1063, 1949.
27. T. Mitsui and J. Furuichi, "Domain structure of rochelle salt and  $\text{KH}_2\text{PO}_4$ ," *Phys. Rev.* **90**(2), pp. 193–202, 1953.
28. W. Zhang and K. Bhattacharya, "A computational model of ferroelectric domains. Part I: Model formulations and domain switching," *Acta. Mater.* **53**, pp. 185–198, 2005.

29. C. Landis, "A new finite-element formulation for electromechanical boundary value problems," *Int. J. Numer. Meth. Eng.* , 2002.
30. E. Fried and M. Gurtin, "Dynamic solid-solid transitions with phase characterized by an order parameter," *Physica D* **72**, pp. 287–308, 1994.
31. W. Zhang and K. Bhattacharya, "A computational model of ferroelectric domains: Part II: Grain boundaries and defect pinning," *Acta Mater.* **53**(1), pp. 199–209, 2005.
32. B. Meyer and D. Vanderbilt, "*Ab initio* study of ferroelectric domain walls in  $\text{PbTiO}_3$ ," *Phys. Rev. B* **65**, pp. 104111–1–104111–11, 2002.